

Contents lists available at [ScienceDirect](http://www.sciencedirect.com)

Journal of Biomechanics

journal homepage: www.elsevier.com/locate/jbiomech
www.JBiomech.com

On arterial fiber dispersion and auxetic effect



K.Y. Volokh

Faculty of Civil and Environmental Engineering, Technion, Haifa, Israel

ARTICLE INFO

Article history:
Accepted 11 July 2017

ABSTRACT

There are two polar contemporary approaches to the constitutive modeling of arterial wall with anisotropy induced by collagen fibers. The first one is based on the angular integration (AI) of the strain energy on a unit sphere for the analytically defined fiber dispersion. The second one is based on the introduction of the generalized structure tensors (GST). AI approach is very involved computationally while GST approach requires somewhat complicated procedure for the exclusion of compressed fibers.

We present some middle ground models, which are based on the use of 16 and 8 structure tensors. These models are moderately involved computationally and they allow excluding compressed fibers easily. We use the proposed models to study the role of the fiber dispersion in the constitutive modeling of the arterial wall. Particularly, we study the *auxetic* effect which can appear in anisotropic materials. The effect means thickening of the tissue in the direction perpendicular to its stretching. Such an effect was not observed in experiments while some simple anisotropic models do predict it. We show that more accurate account of the fiber dispersion suppresses the auxetic effect in a qualitative agreement with experimental observations.

© 2017 Elsevier Ltd. All rights reserved.

1. Introduction

Collagen fibers variously dispersed in soft ground matrix induce anisotropy in the arterial wall. To account for anisotropy within non-linear elasticity [Chuong and Fung \(1983\)](#) generalized the approach of anisotropic linear elasticity by introducing the exponential strain energy function with the Green strain tensor instead of the linearized strain tensor. Since then, various constitutive models of arteries were proposed, e.g. [Takamizawa and Hayashi \(1987\)](#), [Hayashi \(1993\)](#); [Humphrey \(1999\)](#) and others. We note that Fung's approach requires a special choice of the reference coordinates with respect to the characteristic material directions. Instead, frame-invariant formulations of anisotropic finite elasticity can be based on the introduction of the so-called structure tensors, which are presented by tensor products of vectors in the characteristic directions of anisotropy, e.g. [Holzapfel et al. \(2000, 2005\)](#) and [Zulliger et al. \(2004\)](#); and many others recently reviewed by [Holzapfel and Ogden \(2010\)](#). Some relationships between these seemingly different Fung's and frame-invariant formulations were explored by [Ateshian and Costa \(2009\)](#), for example.

Alternatively to Fung's approach, [Lanir \(1983\)](#) (see also [Ehret et al., 2009](#); [Federico and Gasser, 2010](#); [Kassab and Sacks, 2016](#); [Sáez et al., 2016](#); [Gizzi et al., 2016](#)) suggested to account for anisotropy by considering angular dispersion of collagen fibers defined

analytically. This approach is physically appealing yet it generally requires a numerical angular integration (AI) procedure on a unit sphere. Unfortunately, hundreds or, even, thousands integration points on the unit sphere are necessary to provide accuracy of the model. Such integration must be done at every Gauss point of the finite element mesh on every loading step. Thus, the AI approach is very involved computationally. In the attempt to keep the information about the fiber dispersion yet to reduce its computational cost, an approach of the generalized structure tensors (GST) was introduced by [Freed et al. \(2005\)](#) and [Gasser et al. \(2006\)](#). The idea of the GST approach is to account for the fiber dispersion in a structure tensor rather than in the strain energy directly. The latter means that the numerical integration has to be done only once for computing the components of the generalized structure tensors. Once computed these tensors do not change in stress analyses in contrast to the AI approach, in which energy should be perpetually recomputed. Unluckily, the GST approach has its own pitfalls related with the exclusion of the compressed collagen fibers: [Federico and Herzog \(2008\)](#), [Cortes et al. \(2010\)](#), [Pandolfi and Vasta \(2012\)](#), [Holzapfel and Ogden \(2015\)](#), [Lanir and Namani \(2015\)](#), [Melnik et al. \(2015\)](#), [Li et al. \(2016\)](#), [Latorre and Montáns \(2016\)](#) and [Holzapfel and Ogden \(2017\)](#).

In the present work, we make an attempt to keep the advantages of the fiber dispersion models avoiding numerical complications inherent in them. That can be done, in our opinion, by using multiple yet moderate number of structure tensors whose choice reflects upon the collagen structure of the arterial wall. Such an

E-mail address: cvolokh@technion.ac.il

approach is not involved computationally and it allows for an easy exclusion of the collagen fibers in compression. We use the proposed models to study the role of the fiber dispersion in the constitutive modeling of the arterial wall. Particularly, we study the *auxetic* effect which can appear in anisotropic materials. The effect means thickening of the tissue in the direction perpendicular to its stretching. Such an effect was not observed in experiments while some simple anisotropic models do predict it. We show that more accurate account of the fiber dispersion suppresses the auxetic effect in a qualitative agreement with experimental observations.

2. Analytical formulation of the fiber dispersion models

Following the approach of continuum mechanics (Holzapfel, 2000; Volokh, 2016) we substitute the discrete atomic or molecular structure of materials with a continuous set of material particles. A particle placed at \mathbf{x} in the reference configuration Ω_0 moves to position $\mathbf{y}(\mathbf{x})$ in the current configuration Ω . The deformation in the vicinity of the material points is described by the deformation gradient

$$\mathbf{F} = \text{Grady}(\mathbf{x}), \quad (1)$$

or, in Cartesian coordinates: $F_{ij} = \partial y_i / \partial x_j$.

In the absence of body and inertia forces the stress tensor obeys the linear momentum balance in Ω_0 as follows

$$\text{Div} \mathbf{P} = \mathbf{0}, \quad (2)$$

where \mathbf{P} is the first Piola-Kirchhoff stress tensor and $(\text{Div} \mathbf{P})_i = \partial P_{ij} / \partial x_j$ in Cartesian coordinates.

The linear momentum balance on the boundary $\partial \Omega_0$ presents the natural boundary condition

$$\mathbf{P} \mathbf{n} = \bar{\mathbf{t}}, \quad (3)$$

where \mathbf{n} is the unit outward normal to $\partial \Omega_0$ and $\bar{\mathbf{t}}$ is a prescribed referential traction on the boundary.

Alternatively, the essential boundary condition on placements can be prescribed

$$\mathbf{y} = \bar{\mathbf{y}}. \quad (4)$$

We further assume that material is hyperelastic and it is composed of the isotropic ground matrix with the strain energy g and the embedded dispersed collagen fibers with the strain energy f . Then, the first Piola-Kirchhoff stress tensor can be defined by the following constitutive equation

$$\mathbf{P} = -p \mathbf{F}^{-T} + 2 \mathbf{F} \frac{\partial g}{\partial \mathbf{C}} + 2 \mathbf{F} \frac{\partial f}{\partial \mathbf{C}}, \quad (5)$$

where $\mathbf{F}^{-T} \equiv (\mathbf{F}^{-1})^T$; p is the unknown Lagrange multiplier enforcing the incompressibility condition: $\det \mathbf{F} = 1$; and

$$\mathbf{C} = \mathbf{F}^T \mathbf{F} \quad (6)$$

is the right Cauchy-Green tensor.

The strain energy function of the dispersed fibers f is defined by

$$f = \int \rho(\mathbf{a}) w(\lambda(\mathbf{a})) dA, \quad (7)$$

where the integration is on the unit sphere and A is the solid angle; $\rho(\mathbf{a})$ is the angular density of the fiber distribution normalized as follows

$$\int \rho(\mathbf{a}) dA = 4\pi, \quad (8)$$

and $w(\lambda(\mathbf{a}))$ is the strain energy density (per unit reference volume) of an individual fiber as a function of its stretch

$$\lambda(\mathbf{a}) = |\mathbf{F} \mathbf{a}| = \sqrt{\mathbf{a} \cdot \mathbf{C} \mathbf{a}} \geq 1. \quad (9)$$

Here the generic material fiber direction

$$\mathbf{a}(\Phi, \Theta) = \cos \Phi \sin \Theta \mathbf{e}_1 + \sin \Phi \sin \Theta \mathbf{e}_2 + \cos \Theta \mathbf{e}_3, \quad (10)$$

is expressed in spherical coordinates

$$0 \leq \Phi \leq 2\pi, \quad 0 \leq \Theta \leq \pi. \quad (11)$$

Differentiating the strain energy function w with respect to the right Cauchy-Green tensor we obtain the constitutive law in the form

$$\mathbf{P} = -p \mathbf{F}^{-T} + 2 \mathbf{F} \frac{\partial g}{\partial \mathbf{C}} + \int_0^\pi \int_0^{2\pi} \frac{\rho}{\lambda} \frac{\partial w}{\partial \lambda} \mathbf{F} \mathbf{a} \otimes \mathbf{a} \sin \Theta d\Theta d\Phi, \quad (12)$$

or, in terms of the Cauchy stress,

$$\boldsymbol{\sigma} = \mathbf{P} \mathbf{F}^T = -p \mathbf{1} + 2 \mathbf{F} \frac{\partial g}{\partial \mathbf{C}} \mathbf{F}^T + \int_0^\pi \int_0^{2\pi} \frac{\rho}{\lambda} \frac{\partial w}{\partial \lambda} \mathbf{F} \mathbf{a} \otimes \mathbf{F} \mathbf{a} \sin \Theta d\Theta d\Phi, \quad (13)$$

where $\mathbf{1}$ is a second-order identity tensor and the incompressibility condition $\det \mathbf{F} = 1$ has been taken into account.

Remark 1. Following the general trend in the literature, we assumed that collagen fibers did not resist compression. In the case of an individual fiber such assumption is evident, of course. It is less evident when bundles of collagen fibers embedded in the ground matrix are considered. Structurally integrated fibers might resist compression (e.g. Bellini et al., 2014). To understand the mechanical behavior of collagen fibers better it would be interesting to test artery specimens with eliminated ground matrix, if possible. The very existence of the structurally integrated collagen fiber net after the “suppression” of the ground matrix might be a qualitative argument in favor of the collagen resistance to compression.

3. Specialization of the fiber dispersion and strain energies

Further specialization of the theory presented in the previous section requires choice of g , ρ , and w .

It is common to use the neo-Hookean material model for the ground matrix

$$g = \frac{c}{2} (I_1 - 3), \quad (14)$$

where c is the shear modulus of the ground matrix and $I_1 = \text{tr} \mathbf{C}$ is the first principal invariant of \mathbf{C} .

For the fiber dispersion function ρ , we choose the model of a human artery adventitia following Holzapfel et al. (2015) based on experiments by Schriefel et al. (2012)

$$\rho(\Phi, \Theta) = \rho_{\text{op}}(\Theta) \rho_{\text{ip}}(\Phi), \quad (15)$$

where

$$\rho_{\text{op}}(\Theta) = 2 \sqrt{\frac{2b \exp[-2b \cos^2 \Theta]}{\pi \text{erf}(\sqrt{2b})}}, \quad 0 \leq \Theta \leq \pi, \quad (16)$$

and

$$\begin{aligned} \rho_{\text{ip}}(\Phi) &= \frac{1}{2} (\rho_{\text{ip}}^I + \rho_{\text{ip}}^{II}), \\ \rho_{\text{ip}}^I &= \frac{\exp[a \cos 2(\Phi - \alpha)]}{I_0(a)}, \quad 0 \leq \Phi - \alpha \leq 2\pi, \\ \rho_{\text{ip}}^{II} &= \frac{\exp[a \cos 2(\Phi - (\pi - \alpha))]}{I_0(a)}, \quad 0 \leq \Phi - (\pi - \alpha) \leq 2\pi. \end{aligned} \quad (17)$$

Here $\rho_{ip}(\Phi)$ and $\rho_{op}(\Theta)$ describe the in-plane and out-of-plane dispersions, accordingly; a and b are material constants; α is the angle between the mean fiber direction and the circumferential direction \mathbf{e}_1 ;

$$I_0(a) = \frac{1}{\pi} \int_0^\pi \exp[a \cos x] dx \quad (18)$$

is the modified Bessel function of the first kind of order 0; and the error function is defined as

$$\text{erf}(\sqrt{2b}) = \frac{2}{\sqrt{\pi}} \int_0^{\sqrt{2b}} \exp[-x^2] dx. \quad (19)$$

We note that Φ is the angle in the tangent plane, defined by local unit vectors \mathbf{e}_1 and \mathbf{e}_2 , of artery measured from the circumferential direction \mathbf{e}_1 ; and Θ is the out-of-plane angle measured from the radial direction \mathbf{e}_3 – Fig. 1.

The reader should not miss that Holzzapfel et al. (2015) used angle $\pi/2 - \Theta$ instead of Θ used in the present work.

Figs. 2 and 3 present the out-of-plane and in-plane distribution densities with the following dispersion parameters

$$\alpha = 47.99^\circ, \quad a = 2.54, \quad b = 19.44. \quad (20)$$

Finally, we choose the strain energy function of the individual fiber in the form (Holzapfel et al., 2000)

$$w = \frac{k_1}{2k_2} \{ \exp[k_2(I_4 - 1)^2] - 1 \}, \quad (21)$$

where k_1, k_2 are material parameters and

$$I_4 = \mathbf{C} : \mathbf{a} \otimes \mathbf{a} = \lambda(\mathbf{a})^2 \quad (22)$$

is the fourth invariant.

Substitution of the chosen functions in the constitutive law (13) yields

$$\boldsymbol{\sigma} = -p\mathbf{1} + c\mathbf{B} + \int_0^\pi \int_0^{2\pi} \rho_{op}\rho_{ip}\omega\mathbf{F}\mathbf{a} \otimes \mathbf{F}\mathbf{a} \sin \Theta d\Theta d\Phi, \quad (23)$$

where

$$\omega = k_1 \{ I_4 - 1 \} \exp[k_2 \{ I_4 - 1 \}^2], \quad (24)$$

and

$$\mathbf{B} = \mathbf{F}\mathbf{F}^T \quad (25)$$

is the left Cauchy-Green tensor.

The braces in (24) can be interpreted as Macaulay brackets to account for the fiber response in tension only

$$\{x\} = \begin{cases} 0, & x < 0 \\ x, & x \geq 0 \end{cases}, \quad (26)$$

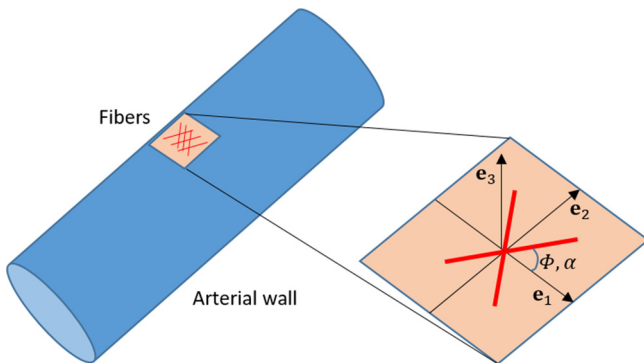


Fig. 1. Local coordinate frame for the arterial wall.

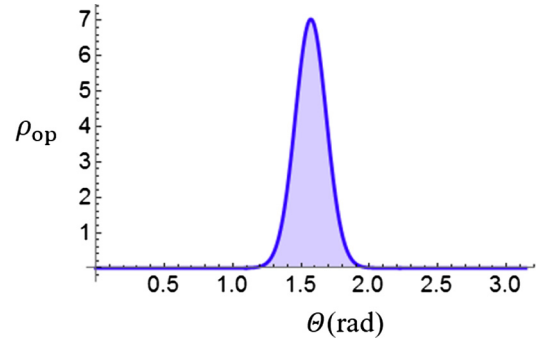


Fig. 2. Out-of-plane fiber dispersion density.

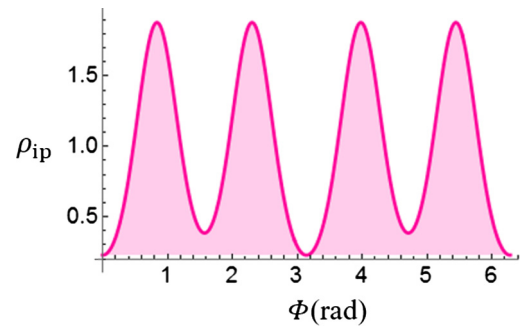


Fig. 3. In-plane fiber dispersion density.

defined, for example, as

$$\{x\} = \frac{1}{2}(x + |x|). \quad (27)$$

4. Dispersion models with multiple structure tensors

Unfortunately, the integrals over the unit sphere can be computed analytically in the very special cases only and, generally, a numerical integration is necessary. The generic formulas allowing for the integration on the sphere are called the cubature formulas. Via the cubature formulas the strain energy density (7) can be rewritten in the form

$$f = \sum_{i=1}^N \beta^{(i)} \rho^{(i)} w^{(i)}, \quad (28)$$

where $\beta^{(i)}$ is a weighting factor and

$$\rho^{(i)} = \rho(\mathbf{a}^{(i)}), \quad w^{(i)} = w(\lambda^{(i)}), \quad \lambda^{(i)} = \lambda(\mathbf{a}^{(i)}) \geq 1, \quad \mathbf{a}^{(i)} = \mathbf{a}(\Phi^{(i)}, \Theta^{(i)}) \quad (29)$$

with N points $(\Phi^{(i)}, \Theta^{(i)})$ chosen on the unit sphere.

Accordingly, the normalization condition (8) reads

$$\sum_{i=1}^N \beta^{(i)} \rho^{(i)} = 4\pi, \quad (30)$$

and the constitutive law (13) takes form

$$\boldsymbol{\sigma} = -p\mathbf{1} + 2\mathbf{F} \frac{\partial g}{\partial \mathbf{C}} \mathbf{F}^T + \sum_{i=1}^N \frac{\beta^{(i)} \rho^{(i)}}{\lambda^{(i)}} \frac{\partial w^{(i)}}{\partial \lambda^{(i)}} \mathbf{F}\mathbf{a}^{(i)} \otimes \mathbf{F}\mathbf{a}^{(i)}. \quad (31)$$

Specializing the fiber dispersion and the strain energies following the previous section we get

$$\boldsymbol{\sigma} = -p\mathbf{1} + c\mathbf{B} + \sum_{i=1}^N \gamma^{(i)} \omega^{(i)} \mathbf{F}\mathbf{a}^{(i)} \otimes \mathbf{F}\mathbf{a}^{(i)}, \quad (32)$$

where

$$\gamma^{(i)} = \beta^{(i)} \rho_{op}^{(i)} \rho_{ip}^{(i)}, \quad \omega^{(i)} = k_1 \{I_4^{(i)} - 1\} \exp[k_2 \{I_4^{(i)} - 1\}^2], \quad (33)$$

and

$$I_4^{(i)} = \mathbf{C} : \mathbf{a}^{(i)} \otimes \mathbf{a}^{(i)}, \quad \rho_{op}^{(i)} = \rho_{op}(\Theta^{(i)}), \quad \rho_{ip}^{(i)} = \rho_{ip}(\Phi^{(i)}). \quad (34)$$

It is important to note that after the application of cubature formulas the general fiber dispersion model can be interpreted as a model based on multiple structure tensors. Indeed, we can consider dyads $\mathbf{a}^{(i)} \otimes \mathbf{a}^{(i)}$, and their “push-forward” to the current configuration $\mathbf{F}\mathbf{a}^{(i)} \otimes \mathbf{F}\mathbf{a}^{(i)}$, at integration points as structure tensors given by the characteristic direction $\mathbf{a}^{(i)}$.

The choice of the integration scheme and, consequently, structure tensors is by no means unique or trivial. In the following subsections we will consider four models. The first one is based on the 21 integration points on the unit sphere following the Bazant and Oh (1986) scheme. The second and third ones are proposed in the present work and they are based on 16 and 8 structures tensors respectively. The difference between the second and third models is that the former accounts for the out-of-plane fiber dispersion while the latter does not. The fourth is the HGO model (Holzapfel et al., 2000) including only two structure tensors.

4.1. Bazant and Oh model with 21 structure tensors

Bazant and Oh (1986) proposed a number of integration schemes on a unit sphere. The most popular and simple one is the 42-point integration scheme, which is summarized in Table 1 for out-of-plane and in-plane angular densities. This scheme is reduced to 21 points with account of symmetry.

A way to control the efficiency of the proposed angular integration scheme is to check the numerical normalization condition (30). Substituting for (30) from Table 1 we compute the following result

$$\sum_{i=1}^{21} \beta^{(i)} \rho_{op}^{(i)} \rho_{ip}^{(i)} = 1.28. \quad (35)$$

This value is unacceptably far from the necessary 4π , which means failure of the integration scheme. This result shows that large numbers of integration points are necessary to catch the anisotropy via AI models. Such conclusion is also in a qualitative cor-

respondence with results of Alastrue et al. (2009a, 2009b) who showed that in the case of anisotropy large number of the integration points on the unit sphere is necessary. Forsell et al. (2013) used from $N = 240$ to $N = 4322$ integration points to describe anisotropy reasonably well.

In summary, from hundreds to thousands integration points on a unit sphere are necessary to use the physically appealing AI models. That is a truly high cost in view of the fact that such integration must be done at every Gauss point of the finite element mesh on every loading step.

4.2. Model with 16 structure tensors with out-of-plane fiber dispersion

Motivated by computational expenses of the traditional AI model, we present here its reduced version based on a moderate number of structure tensors or, equivalently, integration points on the unit sphere. Our main idea is that the general angular integration methods are expensive because they are **universal**. However, the fiber dispersion functions are **specific** and the latter should be taken into account during angular integration. Actually, the dispersion densities are computationally attractive because they are collections of hat-like patterns comprising ascending and descending branches of highly smooth monotonic functions. The latter qualitative notion suggests the idea to use the one-point Gauss integration for every segment (solid angle) of the mesh where fiber dispersion is nonzero.

For example, we partition the sphere as shown in Table 2, where symmetry has been taken into account and the angular ranges for A_i are defined in the second and third columns of the table.

The fourth and fifth columns of this same table give the angular coordinates of the Gauss points on the sphere segments; the sixth column provides their integration weights; the seventh and eighth columns provide the dispersion densities at the Gauss points.

We note that the weight functions are computed as follows

$$\beta^{(i)} = 2 \sin \Theta^{(i)} \Delta \Phi^{(i)} \Delta \Theta^{(i)}, \quad (36)$$

where factor 2 is necessary to account for the symmetry of the integration points in the interval $180^\circ \leq \Delta \Phi^{(i)} \leq 360^\circ$, which was not included in the Table 2; $\Delta \Phi^{(i)}$ and $\Delta \Theta^{(i)}$ are the lengths (in radians) of the corresponding segments given in columns 2 and 3 of Table 2.

To control the quality of the discretization we compute the normalization condition

Table 1
Bazant and Oh 21-point model.

i	$a_1^{(i)}$	$a_2^{(i)}$	$a_3^{(i)}$	$\Theta^{(i)}$ (rad)	$\Phi^{(i)}$ (rad)	$\beta^{(i)}$	$\rho_{op}^{(i)}$	$\rho_{ip}^{(i)}$
1	0.0	0.0	1.0	0.0	0.0	0.053	0	0.226243
2	0.707	0.0	0.707	0.786	0.0	0.040	0	0.226243
3	1.0	0.0	0.0	1.571	0.0	0.053	7.03586	0.226243
4	0.836	0.388	0.388	1.172	0.435	0.050	0.0200111	0.874887
5	0.388	0.388	0.836	0.581	0.785	0.050	0	1.8546
6	0.707	0.707	0.0	1.571	0.786	0.040	7.03586	1.85558
7	0.388	0.836	0.388	1.172	1.136	0.050	0.0200111	1.23005
8	0.0	0.707	0.707	0.786	1.571	0.040	0	0.38408
9	0.0	1.0	0.0	1.571	1.571	0.053	7.03586	0.38408
10	-0.388	0.836	0.388	1.172	2.006	0.050	0.0200111	1.23141
11	-0.707	0.707	0.0	1.571	2.356	0.040	7.03586	1.85518
12	-0.388	0.388	0.836	0.581	2.357	0.050	0	1.8542
13	-0.836	0.388	0.388	1.172	2.707	0.050	0.0200111	0.87363
14	-0.707	0.0	0.707	0.786	3.142	0.040	0	0.226244
15	-0.836	-0.388	0.388	1.172	3.577	0.050	0.0200111	0.876145
16	-0.388	-0.388	0.836	0.581	3.927	0.050	0	1.855
17	-0.388	-0.836	0.388	1.172	4.278	0.050	0.0200111	1.22869
18	0.0	-0.707	0.707	0.786	4.712	0.040	0	0.384081
19	0.388	-0.836	0.388	1.172	5.147	0.050	0.0200111	1.22943
20	0.388	-0.388	0.836	0.581	5.498	0.050	0	1.85478
21	0.836	-0.388	0.388	1.172	5.848	0.050	0.0200111	0.875459

Table 2
Model with 16 structure tensors.

A_i	$\Delta\Phi^{(i)}$	$\Delta\Theta^{(i)}$	$\Phi^{(i)}$	$\Theta^{(i)}$	$\beta^{(i)}$	$\rho_{op}^{(i)}$	$\rho_{ip}^{(i)}$	$\gamma^{(i)} = \beta^{(i)} \rho_{op}^{(i)} \rho_{ip}^{(i)}$
A_1	[0°, 20°]	[75°, 90°]	10°	82.5°	0.181207	3.62778	0.321159	0.211123
A_2	[20°, 48°]	[75°, 90°]	34°	82.5°	0.25369	3.62778	1.40162	1.28996
A_3	[48°, 70°]	[75°, 90°]	59°	82.5°	0.199328	3.62778	1.57071	1.13581
A_4	[70°, 90°]	[75°, 90°]	80°	82.5°	0.181207	3.62778	0.528086	0.347153
A_5	[90°, 110°]	[75°, 90°]	100°	82.5°	0.181207	3.62778	0.528086	0.347153
A_6	[110°, 132°]	[75°, 90°]	121°	82.5°	0.199328	3.62778	1.57071	1.13581
A_7	[132°, 160°]	[75°, 90°]	146°	82.5°	0.25369	3.62778	1.40162	1.28996
A_8	[160°, 180°]	[75°, 90°]	170°	82.5°	0.181207	3.62778	0.321159	0.211123
A_9	[0°, 20°]	[90°, 105°]	10°	97.5°	0.181207	3.62778	0.321159	0.211123
A_{10}	[20°, 48°]	[90°, 110°]	34°	97.5°	0.25369	3.62778	1.40162	1.28996
A_{11}	[48°, 70°]	[90°, 110°]	59°	97.5°	0.199328	3.62778	1.57071	1.13581
A_{12}	[70°, 90°]	[90°, 110°]	80°	97.5°	0.181207	3.62778	0.528086	0.347153
A_{13}	[90°, 110°]	[90°, 110°]	100°	97.5°	0.181207	3.62778	0.528086	0.347153
A_{14}	[110°, 132°]	[90°, 110°]	121°	97.5°	0.199328	3.62778	1.57071	1.13581
A_{15}	[132°, 160°]	[90°, 110°]	146°	97.5°	0.25369	3.62778	1.40162	1.28996
A_{16}	[160°, 180°]	[90°, 110°]	170°	97.5°	0.181207	3.62778	0.321159	0.211123

$$\sum_{i=1}^{16} \beta^{(i)} \rho_{op}^{(i)} \rho_{ip}^{(i)} = \sum_{i=1}^{16} \gamma^{(i)} = 11.94. \tag{37}$$

It is still not the analytically expected 4π yet we observe a dramatic improvement as compared to the universal integration scheme presented in the previous sub-section. It should also be noted that we use only 16 structure tensors instead of 21 in the previous sub-section. Thus, a physically reasonable integration scheme should be used instead of a universal formal rule. We emphasize that the normalization condition is a test for the accuracy of the representation of anisotropy. The closer the result to 4π the better is the approximation. Of course, the reader might further improve the accuracy at the expense of more accurate integration schemes with more structure tensors. We do not do that in the present work.

Remark 2. We should note that the partition presented in Table 2 has been done by trials-and-errors and neglecting some intervals where $\rho_{op} \rightarrow 0$. It is hoped that the readers might find a more formal procedure. Such formalization, if successful, could be important far beyond the topic of the present work.

4.3. Model with 8 structure tensors without out-of-plane fiber dispersion

In the previous sub-section, we made account of the out-of-plane dispersion by partitioning the corresponding density function into two - columns 3 and 5 of Table 2. In the present subsection, we condense the out-of-plane dispersion into the tangent plane as shown in Table 3.

The normalization condition is calculated as follows

$$\sum_{i=1}^8 \beta^{(i)} \rho_{op}^{(i)} \rho_{ip}^{(i)} = \sum_{i=1}^8 \gamma^{(i)} = 12.45, \tag{38}$$

Table 3
Model with 8 structure tensors.

A_i	$\Delta\Phi^{(i)}$	$\Delta\Theta^{(i)}$	$\Phi^{(i)}$	$\Theta^{(i)}$	$\beta^{(i)}$	$\rho_{op}^{(i)}$	$\rho_{ip}^{(i)}$	$\gamma^{(i)} = \beta^{(i)} \rho_{op}^{(i)} \rho_{ip}^{(i)}$
A_1	[0°, 20°]	[82°, 98°]	10°	90°	0.194955	7.03588	0.321159	0.440527
A_2	[20°, 48°]	[82°, 98°]	34°	90°	0.272937	7.03588	1.40162	2.6916
A_3	[48°, 70°]	[82°, 98°]	59°	90°	0.214451	7.03588	1.57071	2.36997
A_4	[70°, 90°]	[82°, 98°]	80°	90°	0.194955	7.03588	0.528086	0.724365
A_5	[90°, 110°]	[82°, 98°]	100°	90°	0.194955	7.03588	0.528086	0.724365
A_6	[110°, 132°]	[82°, 98°]	121°	90°	0.214451	7.03588	1.57071	2.36997
A_7	[132°, 160°]	[82°, 98°]	146°	90°	0.272937	7.03588	1.40162	2.6916
A_8	[160°, 180°]	[82°, 98°]	170°	90°	0.194955	7.03588	0.321159	0.440527

and its value is reasonably good.

This model is essentially simple and accurate for the in-plane fiber dispersion. Actually, the models with the in-plane fiber dispersion dominate the literature and it will be instructive to use the presented model in the subsequent computations.

4.4. Holzapfel-Gasser-Ogden model with 2 structure tensors

In addition to the models presented in the previous subsections we take the HGO model (Holzapfel et al., 2000) as a limit with two structure tensors only. In the latter case there is no fiber dispersion and we set

$$\gamma^{(1)} = \gamma^{(2)} = 1, \tag{39}$$

and

$$\Theta^{(1)} = \Theta^{(2)} = 90^\circ, \quad \Phi^{(1)} = 47.99^\circ, \quad \Phi^{(2)} = 132.01^\circ. \tag{40}$$

Obviously, the fiber dispersion is completely ‘condensed’ in material constants k_1 and k_2 in this case.

5. Uniaxial tension in circumferential and axial directions

In this section we examine the models considered above in the cases of uniaxial tension in circumferential and axial directions of an artery.

Deformation is prescribed in the form

$$\mathbf{F} = \lambda_1 \mathbf{e}_1 \otimes \mathbf{e}_1 + \lambda_2 \mathbf{e}_2 \otimes \mathbf{e}_2 + \lambda_1^{-1} \lambda_2^{-1} \mathbf{e}_3 \otimes \mathbf{e}_3, \tag{41}$$

where in-plane stretches of the arterial wall λ_1 and λ_2 are independent and the out-of-plane stretch is derived from the incompressibility condition: $\lambda_3 = \lambda_1^{-1} \lambda_2^{-1}$.

In this case, the fourth (pseudo-) invariant of the i -th structure tensor is

$$I_4^{(i)} = (\lambda_1 \cos \Phi^{(i)} \sin \Theta^{(i)})^2 + (\lambda_2 \sin \Phi^{(i)} \sin \Theta^{(i)})^2 + (\lambda_1^{-1} \lambda_2^{-1} \cos \Theta^{(i)})^2. \tag{42}$$

The principal stresses coincide with the local coordinate axes and they can be written as follows

$$\begin{aligned} \sigma_1 &= -p + c\lambda_1^2 + \sum_{i=1}^N \gamma^{(i)} \omega^{(i)} \lambda_1^2 \cos^2 \Phi^{(i)} \sin^2 \Theta^{(i)}, \\ \sigma_2 &= -p + c\lambda_2^2 + \sum_{i=1}^N \gamma^{(i)} \omega^{(i)} \lambda_2^2 \sin^2 \Phi^{(i)} \sin^2 \Theta^{(i)}, \\ \sigma_3 &= -p + c\lambda_1^{-2} \lambda_2^{-2} + \sum_{i=1}^N \gamma^{(i)} \omega^{(i)} \lambda_1^{-2} \lambda_2^{-2} \cos^2 \Theta^{(i)}. \end{aligned} \tag{43}$$

Assuming thin layer, $\sigma_3 = 0$, we calculate the unknown Lagrange parameter p and obtain

$$\begin{aligned} \sigma_1 &= c(\lambda_1^2 - \lambda_1^{-2} \lambda_2^{-2}) + \sum_{i=1}^N \gamma^{(i)} \omega^{(i)} (\lambda_1^2 \cos^2 \Phi^{(i)} \sin^2 \Theta^{(i)} - \lambda_1^{-2} \lambda_2^{-2} \cos^2 \Theta^{(i)}), \\ \sigma_2 &= c(\lambda_2^2 - \lambda_1^{-2} \lambda_2^{-2}) + \sum_{i=1}^N \gamma^{(i)} \omega^{(i)} (\lambda_2^2 \sin^2 \Phi^{(i)} \sin^2 \Theta^{(i)} - \lambda_1^{-2} \lambda_2^{-2} \cos^2 \Theta^{(i)}). \end{aligned} \tag{44}$$

Table 4
Calibration of three models.

	c [kPa]	k_1 [kPa]	k_2
Model with 16 structure tensors	5.0	2.23	1.63
Model with 8 structure tensors	5.0	2.04	1.58
HGO model with 2 structure tensors	10.0	7.5	27.5

We emphasize that, contrary to the isotropic case, both stretches λ_1 and λ_2 are independent and must be found from the simultaneous solution of the previous equations.

In particular, in the case of the uniaxial tension in the circumferential direction we have

$$\begin{aligned} \sigma_1(\lambda_1, \lambda_2) &= \sigma, \\ \sigma_2(\lambda_1, \lambda_2) &= 0, \end{aligned} \tag{45}$$

where σ is the Cauchy tension.

Alternatively, in the case of the uniaxial tension in the axial direction we have

$$\begin{aligned} \sigma_1(\lambda_1, \lambda_2) &= 0, \\ \sigma_2(\lambda_1, \lambda_2) &= \sigma. \end{aligned} \tag{46}$$

Based on the experimental data presented in Holzapfel et al. (2015) and using the least squares fit we calibrate the 16-, 8-, and 2- structure tensors models described above as shown in Table 4.

We solve the system of Eqs. (45) and (46) to generate the stress-stretch and stretch-stretch curves presented in Figs. 4–6 for the considered constitutive models.

Remarkably, we observe the ‘auxetic effect’ in the case of the HGO model shown on the bottom right of Fig. 6 where the lateral stretch becomes positive at tension for $\lambda_2 > 1.35$. This effect is not observed in the other models discussed in the range of interest - it is model-dependent!

Remark 3. It is important to emphasize that the experimental data from Holzapfel et al. (2015) used for the calibration does not exactly correspond to the used fiber dispersion data from Schriefel et al. (2012). “Imaging and material data were obtained from different but comparable tissues” (Holzapfel et al., 2015). This

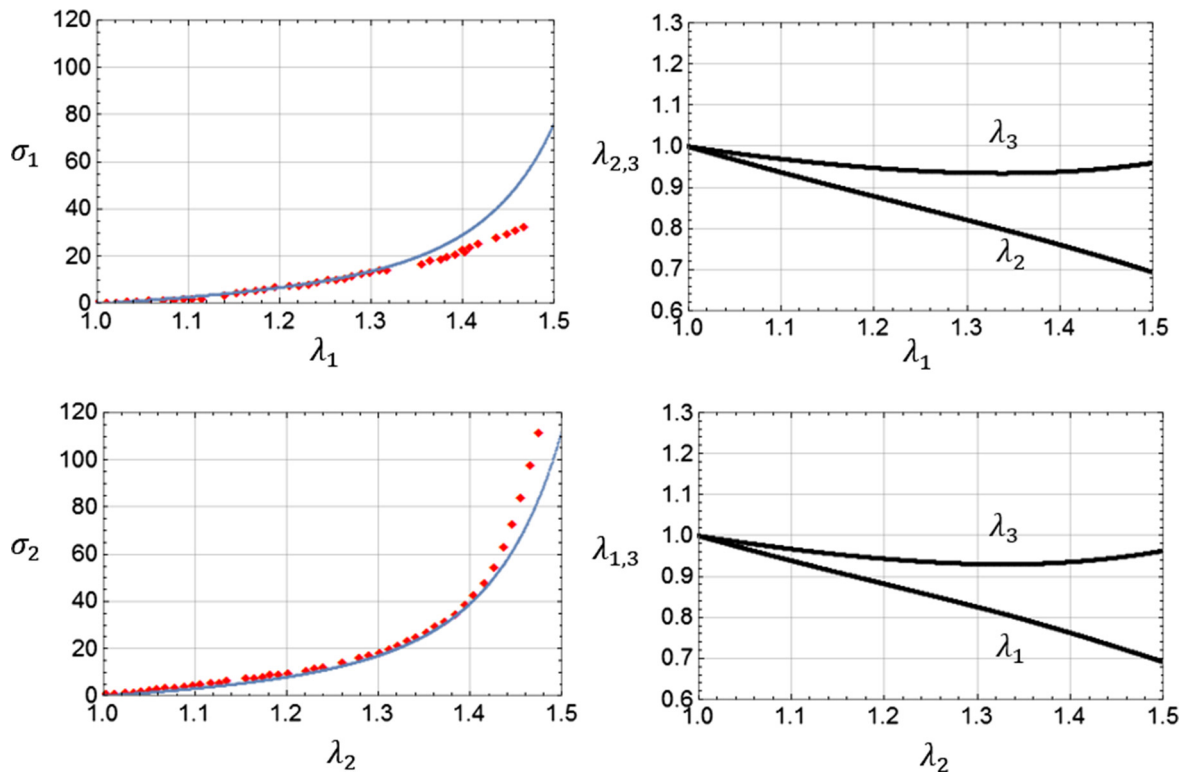


Fig. 4. Uniaxial tension in circumferential (top) and axial (bottom) direction for the 16 structure tensors model. Cauchy stress [kPa] versus stretch in circumferential (left) and lateral stretches (right). Red diamonds show the experimental data. (For interpretation of the references to colour in this figure legend, the reader is referred to the web version of this article.)

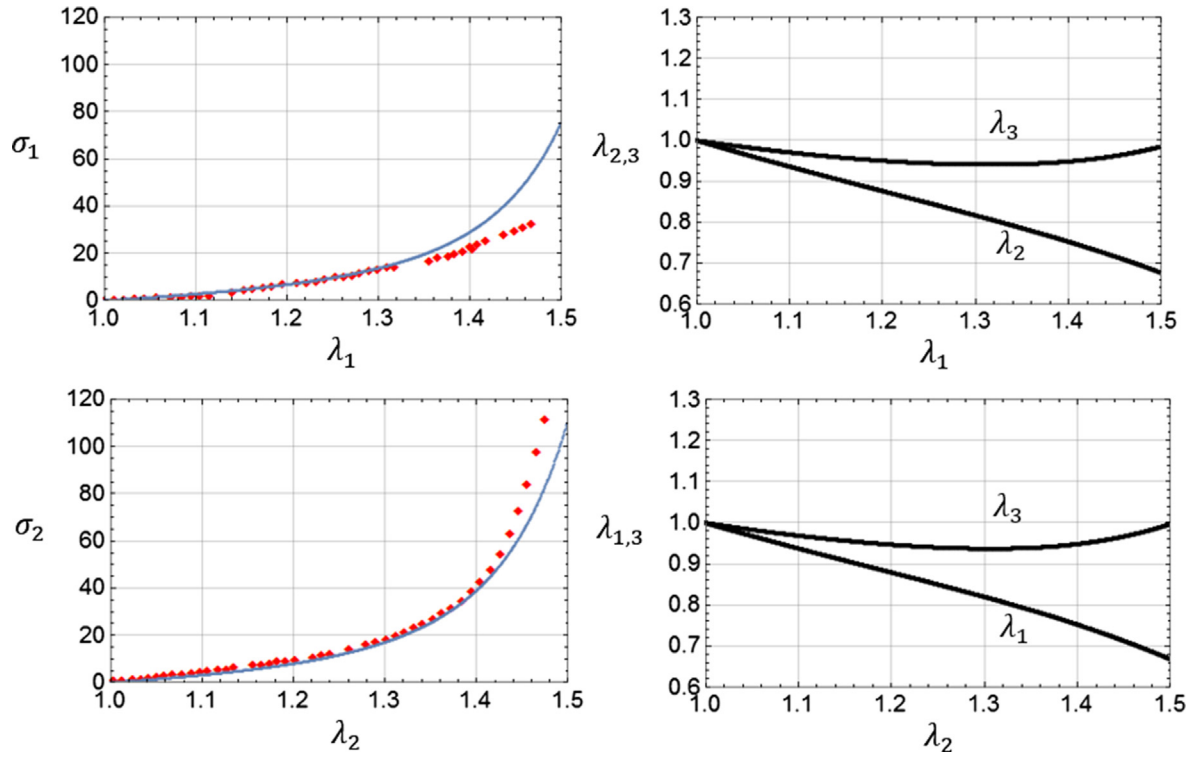


Fig. 5. Uniaxial tension in circumferential (top) and axial (bottom) direction for the 8 structure tensors model. Cauchy stress [kPa] versus stretch in circumferential (left) and lateral stretches (right). Red diamonds show the experimental data. (For interpretation of the references to colour in this figure legend, the reader is referred to the web version of this article.)

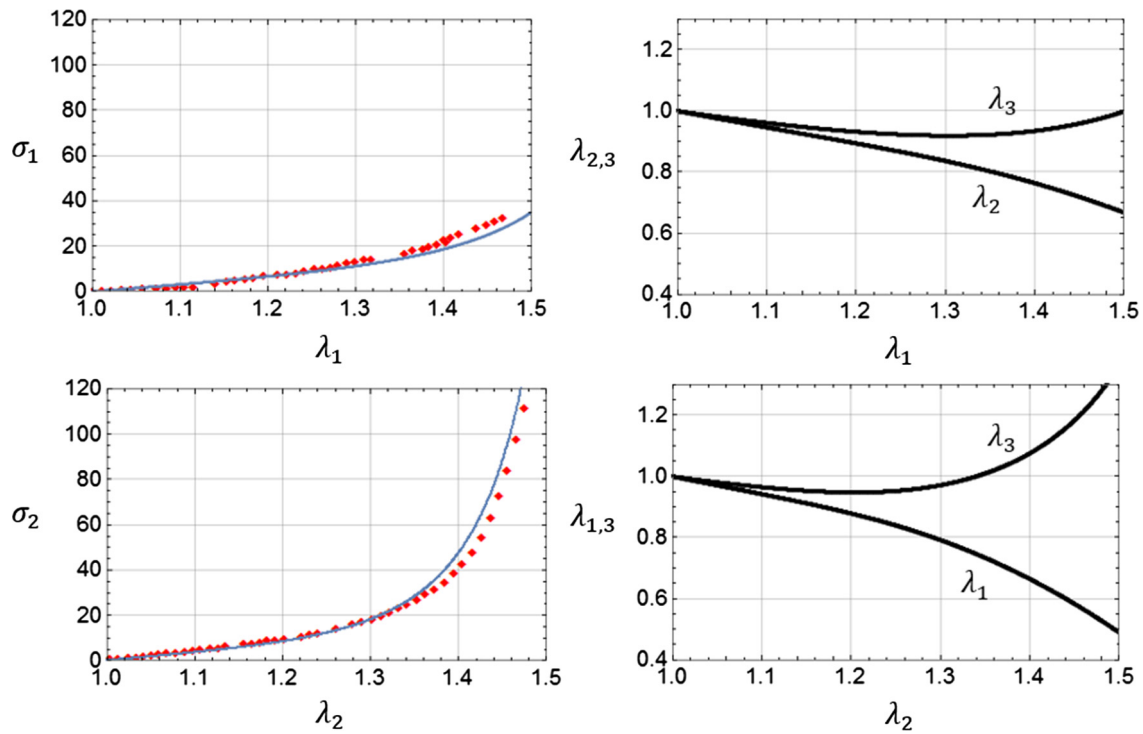


Fig. 6. Uniaxial tension in circumferential (top) and axial (bottom) direction for the HGO model. Cauchy stress [kPa] versus stretch in circumferential (left) and lateral stretches (right). Red diamonds show the experimental data. (For interpretation of the references to colour in this figure legend, the reader is referred to the web version of this article.)

notion can, probably, explain some divergence of the experiment and fiber-dispersion models. It is also interesting that the fiber dispersion ‘smears’ anisotropy as expected intuitively.

6. Conclusion

In this paper, we introduced new constitutive models of the arterial wall, which accounted for the collagen fiber dispersion. We used neither full angular integration (AI) nor generalized structure tensors (GST) popular in the literature. Instead, we used the multiple (16 and 8) structure tensors introduced on the basis of the specific angular distribution of collagen fibers. The introduced models are computationally attractive in contrast to the AI approach and they allow for an easy exclusion of compressed fibers in contrast to the GST approach.

We applied the developed models to analysis of uniaxial tension in circumferential and axial directions of an arterial wall. We found that the proposed models did not exhibit any auxetic effect as was consistent with experiments: Skacel and Bursa (2016), Holzapfel (2017). In contrast to the proposed model, more simple anisotropic model based on 2 structure tensors does predict the auxetic effect - see analyses in Latorre et al. (2016) and Murphy and Biwa (2017). Apparently, the account of the fiber dispersion via multiple structure tensors improves the physical appeal of constitutive modeling.

Conflict of interest

None.

References

- Alastrue, V., Martínez, M.A., Doblare, M., Menzel, A., 2009a. Anisotropic micro-sphere-based finite elasticity applied to blood vessel modelling. *J. Mech. Phys. Solids* 57, 178–203.
- Alastrue, V., Martínez, M.A., Menzel, A., Doblare, M., 2009b. On the use of non-linear transformations for the evaluation of anisotropic rotationally symmetric directional integrals. Application to the stress analysis in fibred soft tissues. *Int. J. Numer. Meth. Eng.* 79, 474–504.
- Ateshian, G.A., Costa, K.D., 2009. A frame-invariant formulation of Fung elasticity. *J. Biomech.* 42, 781–785.
- Bazant, Z.P., Oh, B.H., 1986. Efficient numerical integration on the surface of a sphere. *ZAMM* 66, 37–49.
- Bellini, C., Ferruzzi, J., Roccabianca, S., Di Martino, E.S., Humphrey, J.D., 2014. A microstructurally motivated model of arterial wall mechanics with mechanobiological implications. *Ann. Biomed. Eng.* 42, 488–502.
- Chuong, C.J., Fung, Y.C., 1983. Three-dimensional stress distribution in arteries. *J. Biomech. Eng.* 105, 268–274.
- Cortes, D.H., Lake, S.P., Kadlowec, J.A., Soslowsky, L.J., Elliot, D.M., 2010. Characterizing the mechanical contribution of fiber angular distribution in connective tissue: comparison of two modeling approaches. *Biomech. Model. Mechanobiol.* 9, 651–658.
- Ehret, A.E., Itskov, M., Weinhold, G.W., 2009. A micro mechanically motivated model for the viscoelastic behaviour of soft biological tissues at large strains. *Nuovo Cimento della Società Italiana di Fisica. C, Geophys. Space Phys.* 32, 73–80.
- Federico, S., Gasser, T.C., 2010. Nonlinear elasticity of biological tissues with statistical fibre orientation. *J. Roy. Soc. Interface* 7, 955–966.
- Federico, S., Herzog, W., 2008. Towards an analytical model of soft biological tissues. *J. Biomech.* 41, 3309–3313.
- Forsell, C., Swedenborg, J., Roy, J., Gasser, T.C., 2013. The quasi-static failure properties of the abdominal aortic aneurysm wall estimated by a mixed experimental-numerical approach. *Ann. Biomed. Eng.* 41, 1554–1566.
- Freed, A.D., Einstein, D.R., Vesely, I., 2005. Invariant formulation for dispersed transverse isotropy in aortic heart valves. *Biomech. Model. Mechanobiol.* 4, 100–117.
- Gasser, T.C., Ogden, R.W., Holzapfel, G.A., 2006. Hyperelastic modeling of arterial layers with distributed collagen fibre orientations. *J. R. Soc. Interface* 3, 15–35.
- Gizzi, A., Pandolfi, A., Vastac, M., 2016. Statistical characterization of the anisotropic strain energy in soft materials with distributed fibers. *Mech. Mater.* 92, 119–138.
- Hayashi, K., 1993. Experimental approaches on measuring the mechanical properties and constitutive laws of arterial walls. *J. Biomech. Eng.* 115, 481–488.
- Holzapfel, G.A., 2000. *Nonlinear Solid Mechanics*. Wiley.
- Holzapfel, G.A., 2017. Personal communication.
- Holzapfel, G.A., Gasser, T.C., Ogden, R.W., 2000. A new constitutive framework for arterial wall mechanics and a comparative study of material models. *J. Elast.* 61, 1–48.
- Holzapfel, G.A., Niestrawska, J.A., Ogden, R.W., Reinisch, A.J., Schriefl, A.J., 2015. Modeling non-symmetric collagen fiber dispersion in arterial walls. *J. R. Soc. Interface* 12, 20150188.
- Holzapfel, G.A., Ogden, R.W., 2010. Constitutive modeling of arteries. *Proc. Roy. Soc. A* 466, 1551–1597.
- Holzapfel, G.A., Ogden, R.W., 2015. On the tension–compression switch in soft fibrous solids. *Eur. J. Mech. A/Solids* 49, 561–569.
- Holzapfel, G.A., Ogden, R.W., 2017. On fiber dispersion models: exclusion of compressed fibers and spurious model comparisons. *J. Elast.* (in press).
- Holzapfel, G.A., Sommer, G., Gasser, C.T., Regitnig, P., 2005. Determination of the layer-specific mechanical properties of human coronary arteries with non-atherosclerotic intimal thickening, and related constitutive modeling. *Am. J. Physiol. Heart Circ. Physiol.* 289, H2048–2058.
- Humphrey, J.D., 1999. An evaluation of pseudoelastic descriptors used in arterial mechanics. *J. Biomech. Eng.* 121, 259–262.
- Kassab, G.S., Sacks, M.S., 2016. *Structure-Based Mechanics of Tissues and Organs*. Springer.
- Lanir, Y., 1983. Constitutive equations for fibrous connective tissues. *J. Biomech.* 16, 1–12.
- Lanir, Y., Namani, R., 2015. Reliability of structure tensors in representing soft tissues structure. *J. Mech. Behav. Biomed. Mater.* 46, 222–228.
- Latorre, M., Montáns, F.J., 2016. On the tension–compression switch of the Gasser–Ogden–Holzapfel model: analysis and a new pre-integrated proposal. *J. Mech. Behav. Biomed. Mater.* 57, 175–189.
- Latorre, M., Romero, X., Montáns, F.J., 2016. The relevance of transverse deformation effects in modeling soft biological tissues. *Int. J. Solids Struct.* 99, 57–70.
- Li, K., Ogden, R.W., Holzapfel, G.A., 2016. Computational method for excluding fibers under compression in modeling soft fibrous solids. *Euro J. Mech. A/Solids* 57, 178–193.
- Melnik, A.V., Borja Da Rocha, H., Gorieli, A., 2015. On the modeling of fiber dispersion in fiber-reinforced elastic materials. *Int. J. Non-Linear Mech.* 75, 92–106.
- Murphy, J.G., Biwa, S., 2017. The counter-intuitive mechanical response in simple tension of arterial models that are separable functions of the I1, I4, I6 invariants. *Int. J. Non-Linear Mech.* 90, 72–81.
- Pandolfi, A., Vasta, M., 2012. Fiber distributed hyperelastic modeling of biological tissues. *Mech. Mater.* 44, 151–162.
- Sáez, P., García, A., Peña, E., Gasser, T.C., Martínez, M.A., 2016. Microstructural quantification of collagen fiber orientations and its integration in constitutive modeling of the porcine carotid artery. *Acta Biomater.* 33, 183–193.
- Skacel, P., Bursa, J., 2016. Poisson’s ratio of arterial wall—Inconsistency of constitutive models with experimental data. *J. Mech. Behav. Biomed. Mater.* 54, 316–327.
- Schriefl, A.J., Zeindlinger, G., Pierce, D.M., Regitnig, P., Holzapfel, G.A., 2012. Determination of the layer-specific distributed collagen fiber orientations in human thoracic and abdominal aortas and common iliac arteries. *J. R. Soc. Interface* 9, 1275–1286.
- Takamizawa, K., Hayashi, K., 1987. Strain energy density function and uniform strain hypothesis for arterial mechanics. *J. Biomech.* 20, 7–17.
- Volokh, K.Y., 2016. *Mechanics of Soft Materials*. Springer.
- Zulliger, M.A., Fridez, P., Hayashi, K., Stergiopoulos, N., 2004. A strain energy function for arteries accounting for wall composition and structure. *J. Biomech.* 37, 989–1000.